A Journal of the Gesellschaft Deutscher Chemiker

Angewandte International Edition GDCh Chemie

www.angewandte.org

Accepted Article

Title: Naphthochromenones: Organic Bimodal Photocatalysts Engaging in Both Oxidative and Reductive Quenching Processes.

Authors: Javier Mateos, Francesco Rigodanza, Alberto Vega, Andrea Sartorel, Mirco Natali, Tommaso Bortolato, Giorgio Pelosi, Xavier Companyo, Marcella Bonchio, and Luca Dell'Amico

To be cited as: *Angew. Chem. Int. Ed.* 10.1002/anie.201912455
Angew. Chem. 10.1002/ange.201912455

Link to VoR: http://dx.doi.org/10.1002/anie.201912455
http://dx.doi.org/10.1002/ange.201912455

WILEY-VCH

10.1002/anie.201912455

WILEY-VCH

RESEARCH ARTICLE

Naphthochromenones: Organic Bimodal Photocatalysts Engaging in Both Oxidative and Reductive Quenching Processes.

Javier Mateos,[§[a]] Francesco Rigodanza,[§[a]] Alberto Vega–Peñaloza,[[a]] Andrea Sartorel,[[a]] Mirco Natali, [[b]] Tommaso Bortolato,[[a]] Giorgio Pelosi,[[c]] Xavier Companyó,[[a]] Marcella Bonchio,[[a]] and Luca Dell'Amico*[[a]]

In memory of Dieter Enders (1946–2019) for his invaluable contribution to organic chemistry

Abstract: 12 different naphthochromenone photocatalysts (PCs) have been synthesized at gram–scale, combining absorption features across the UV–Vis spectrum, up to 440 nm with an extremely wide redox window (up to 3.22 eV) that is accessible using simple visible light irradiation sources (CFL or LED). Their excited state redox potentials, PC*/PC$^{\bullet-}$ = up to 1.65 V and PC$^{\bullet+}$/PC* up to –1.77 V vs SCE, are such that these novel PCs can engage in both oxidative and reductive quenching mechanisms with strong thermodynamic requirements. Converging absorption/emission spectroscopy and cyclic voltammetry we delineate robust structure–properties relationships, that are further supported by time–dependent density functional theory (TD–DFT) calculations. The potential of these bimodal PCs has been benchmarked in thermodynamically challenging photocatalytic processes, were strong oxidative (> 1.46 V) and strong reductive power (< –1.96 V) is required. Further advantages are given by their simple recovery and reuse – up to four times, without any significant loss in their photocatalytic performances. The ability of efficiently catalysing mechanistically opposite oxidative/reductive photoreactions is a unique feature for organic photocatalysts. This new class of molecules represents a decisive advancement towards generality, sustainability and cost efficiency in photoredox catalysis.

Introduction

Solar light is an unlimited source of clean and renewable energy on Earth.[1] Its conversion into diverse energy forms is at the forefront of intense research in diverse scientific areas from biology to engineering. The chemical community, playing a central role across disciplines, has devoted enormous efforts in the identification of more efficient photocatalysts (PCs), capable of performing light–driven transformations under catalytic routines.[2] The utilization of these molecules has direct impact on our every–day life, from the synthesis of polymers[3] to the more recent applications towards natural products synthesis or drug development.[4] Recently, the identification of novel photocatalytic systems[5] has become an extremely active filed of research.[6,7]

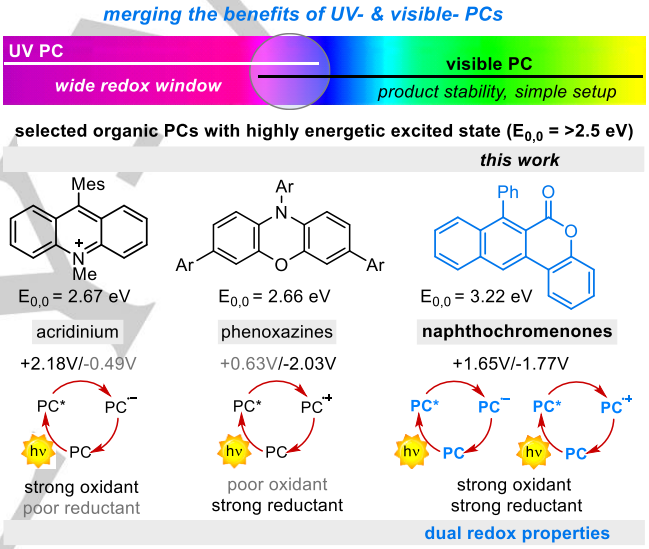

Figure 1. Organic photoredox catalysts (PCs) absorbing between UV– and visible–light (bottom). Mes = mesityl. Ar = 2–naphtyl. Reported redox potentials vs SCE.

New directions are pointing to the identification of more sustainable purely-organic molecules,[8, 5e–g] able to conserve all the advantages of the well-established metal-based PCs (Ru, Ir or Cu complexes),[5a–d] including: i) the use of visible-light photons (≥ 400 nm), abundant in the solar emission spectra and capable of minimizing product decomposition,[2, 5a, b] ii) the use of readily available light sources such as CFL or LED, and finally iii) an equal distribution of the excited state energy among the oxidation and reduction potentials, thus delivering upon light irradiation both a strong oxidant and a strong reductant. This bimodal way of action is rare in organic photocatalysis, especially when connected to high excites state energies ($E_{0,0}$ > 2.5 eV).[5e-g] The large majority of organic PCs with an $E_{0,0}$ > 2.5 eV are able to catalyse either oxidative or reductive photoreactions with extreme thermodynamic requirements (see e.g. acridiniums of phenoxazines in Figure 1),[5e] forcing the user to move from one class of PCs to another one, when changing the operative reaction mechanism. The combination within a single molecule of

[a] J. Mateos, F. Rigodanza, A. Vega–Peñaloza, A. Sartorel, T. Bortolato, X. Companyó, M. Bonchio, L. Dell'Amico
Department of Chemical Sciences
University of Padova Institution
Via Marzolo 1, 35131 Padova, Italy
E–mail: luca.dellamico@unipd.it
[b] M. Natali
Department of Chemical and Pharmaceutical Sciences
University of Ferrara Institution
Via Luigi Borsari 46, 44121 Ferrara, Italy
[c] G. Pelosi
Department of Chemistry, Life Sciences and Environmental Sustainability, University of Parma
Parco Area delle Scienze 17, 43124 Parma, Italy
[§] These authors contributed equally to this work.

Supporting information for this article is given via a link at the end of the document.

10.1002/anie.201912455
WILEY-VCH

RESEARCH ARTICLE

a strong oxidative exited state power (up to 1.5 V), an equally strong reductive power (up to -1.5 V), and an absorption under visible-light (≥ 400 nm), will define an ideal class of bimodal organic PCs, capable of performing both thermodynamically challenging oxidative and reductive processed in a catalytic routine. This class of molecules, having a wider operational window, will impart new mechanistic avenues in photocatalysis.

We herein outline the identification of *6H*–naphthochromen–6–one (NT) as a novel family of bimodal organic PCs (Figure 1, right). NTs present an absorption spectrum at the border of visible–light, which guarantees the access of high energy excited state (up to 3.22 eV) with the use of simple visible light sources, maintaining both strong oxidative and strong reductive properties, E (PC*/PC$^{\bullet-}$) up to 1.65 V and E (PC$^{\bullet+}$/PC*) up to –1.77 V vs SCE. The identification of a scalable synthetic plan together with easy structural functionalisation lead to the generation of 12 diverse PCs at gram scale. Structure–photoredox property relationships are assessed in terms of HOMO–LUMO energy, absorption/emission, ground/excited state potentials, fluorescence quantum yield and excited state lifetime, allowing a rational use to the intended purpose. Remarkably, the potential of this new class of PCs is demonstrated for a variety of mechanistically diverse transformations classically promoted by either UV- or visible-light absorbing PCs. Furthermore, NTs can be easily recovered and reused, up to four runs, in subsequent catalytic cycles with comparable photoredox performances.

Results and Discussion

The identification of the NT scaffold **5** as potential organic PC was stimulated by our previous works on the synthesis of the tetracyclic scaffolds **3**.[9] (Scheme 1). We envisaged compound **3**, derived from the reaction between the photoenol, generated upon light excitation of the corresponding benzophenones **1**,[10] and coumarins **2**, as precursor of NT **5** through an elimination/aromatization sequence (Scheme 1). We must consider that both starting materials benzophenone **1** and coumarin **2** have distinctive absorptions under the UV region.[11] This fact also suggested a possible absorption at longer wavelengths of the more conjugated scaffold **5**. Once identified a general synthetic strategy (Scheme 1), suitable reaction conditions were developed and applied to diverse readily available starting materials **1a**–**c** and **2a**–**c**, allowing the easy tuning of the NT scaffold at positions 3 and 7 (Table 1). The initial light–driven [4+2]–cycloaddition reaction between benzophenone **1a** and coumarin **2a** was performed under microfluidic conditions.[9b] Tetracyclic product **3a** formed rapidly within 35 min residence time. Isolation of **3a** and subsequent treatment with triflic acid delivered directly NT scaffold **5a** without the need of any additional synthetic operation.[12] A simple recrystallization furnished compounds **5a**–**5c** with variations at position 7 in good overall yields 37%–82%.

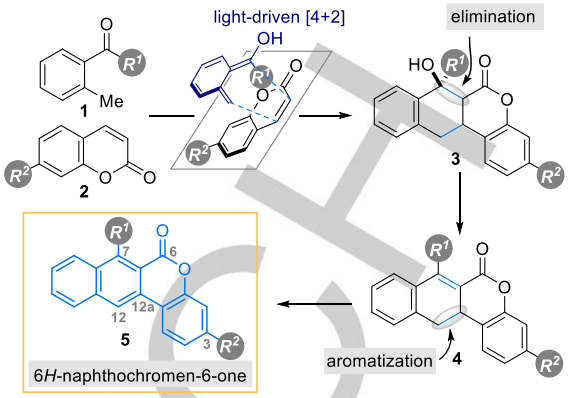

Scheme 1. Synthesis of PCs **5a**–**f** from carbonyl compounds **1a**–**c** and coumarins **2a**–**c**.

We started the synthesis of differently substituted NTs **5**, with the goal of defining structure–property relationships while generating a library of PCs with varied photoredox properties.

Table 1. Synthesis of PCs **5a**–**f** from carbonyl compounds **1a**–**c** and coumarins **2a**–**c**.

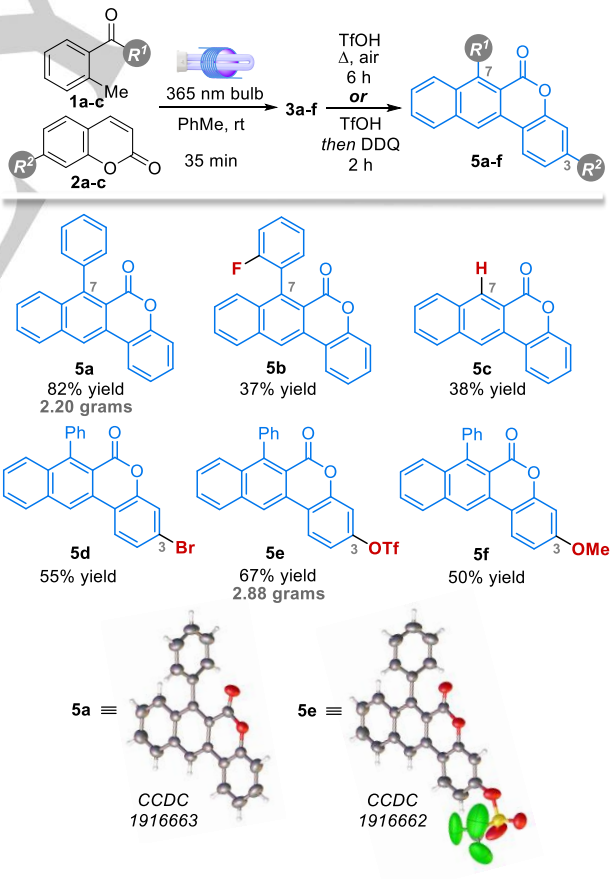

10.1002/anie.201912455
WILEY-VCH

RESEARCH ARTICLE

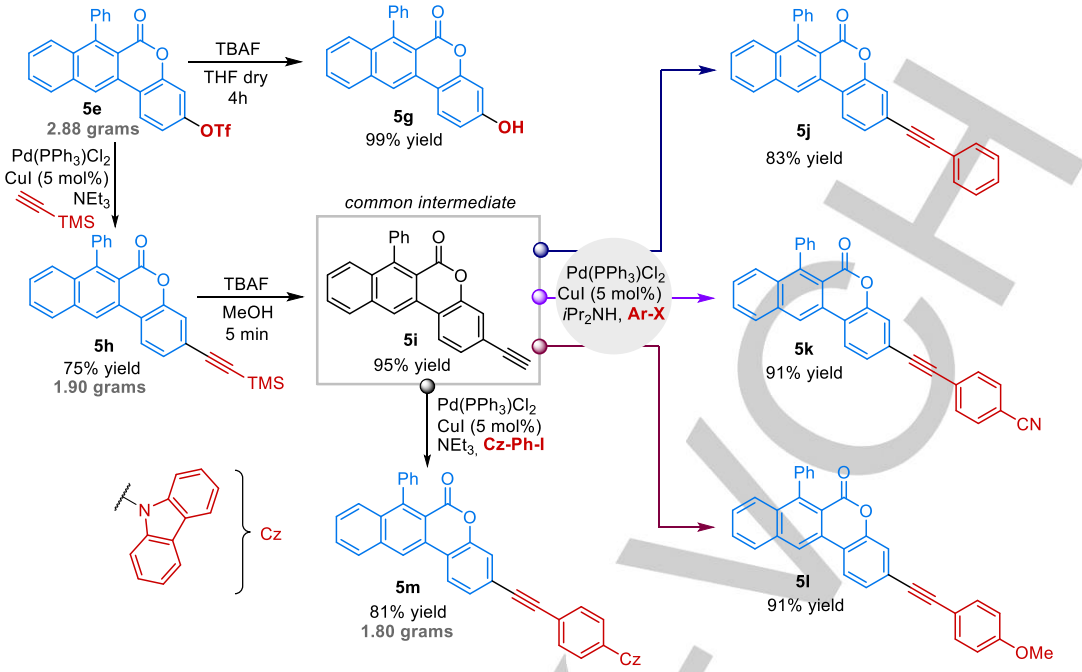

Scheme 2. Post–functionalization of PC **5e** for the synthesis of PCs **5g**,**h** and **5j**–**m**. All the yields refer to isolated yields. TBAF = tetrabutylammonium fluoride. Cz = carbazole. For **5j**–**5l** X = I, for **5k** X = Br.

Compounds **5d**–**5f**, bearing diverse groups at position 3 were synthesized in overall yields spanning from 36% to 67%. In these cases, a two–step elimination–aromatization sequence resulted in improved yields and diminished reaction time (See SI). Remarkably, the developed synthetic protocol was scaled up without any yield drop, producing **5a**, and **5e** at gram scale and up to 2.88 g within 40 h. The structure of **5a** and **5e** were confirmed by X–ray analysis on single crystal. Prompted by the simple synthetic route developed, we explored the impact of diverse structural functionalization. We identified **5e**, bearing an OTf group at position 3, as a versatile precursor to diverse PCs scaffolds. The hydroxyl functionality was easily deprotected with tetrabutylammonium fluoride (TBAF) solution, delivering PC **5g** in quantitative yield (Scheme 2 top, left). Additionally, scaffold **5h** was synthetized (75% yield, 1.90 g) in order to evaluate the effect of an increased conjugation. After a simple desilylation step, **5i** was obtained in high yield (95%) after simple filtration on a silica–pad (Scheme 2, grey box). At this juncture, diverse aromatic substituents bearing electron withdrawing or electron donating groups were introduced by a simple synthetic operation (Scheme 2, right and bottom). PCs **5j**–**5m** were synthesized in excellent yields at gram scale (up to 1.80 g) spanning from 81% to 91% by using **5i** and selected aryl halides through a Sonogashira cross–coupling. With a wide library of novel organic PCs in hand, we next examined their photoredox properties.

Analysis of the Photochemical and Redox Properties. We first looked at the properties of PCs **5** in both the excited and ground states, crucial in effecting the photocatalytic performances. **5a** showed a distinctive absorption spectrum with a peak centred at 380 nm (ε = 5100 $M^{-1}cm^{-1}$) and a shoulder at 360 nm, tailing up to 440 nm (Figure 2a, black line), and three distinct peaks between 300–330 nm (299, 313 and 327 nm). To get insight into the electronic transitions responsible for the absorption, we used time–dependent density functional theory (TD–DFT) at the B3LYP/6–311+g(d,p) level of theory, including a polarizable continuum model in polar solvent.[13] As shown in Figure 2c (black levels), the HOMO, LUMO and LUMO+1 orbitals are localized on the NT core of **5a**, with no contribution of the phenyl group at 7 position.[14] These three orbitals are involved in the two low energy transitions calculated with TD–DFT. In particular, the HOMO→LUMO transition provides the highest contribution (91%, Table S11 in SI) to the lowest energetic one, predicted at 362 nm (Figure 2a, dotted line) and characterized by an oscillator strength of 0.0693 (ε = 5×103 $M^{-1}cm^{-1}$). The second lowest energetic transition is predicted at 323 nm (oscillator strength 0.1848), in excellent agreement with the experimental data, and it is characterised by a major HOMO→LUMO+1 contribution setting to 71%. While substitutions at position 7 have relatively small influence on the PCs absorption spectra (Figure S133 in SI), the introduction of a bromine (**5d**) or a triflate (**5e**) at position 3, is reflected in a slight shift of the peaks at longer wavelengths. Conversely, compounds **5f** and **5g**, bearing electron donating groups have highly enhanced absorption in the visible region, in particular **5f** (Figure 2b, orange line) being the most absorbing in the series of PCs. Interestingly, this behaviour was consistent with calculated absorptions by TD–DFT (Table S11 in SI). Focusing on the two less energetic transitions, significant effects are observed for **5f** and **5g**, where a 0.2–0.3 eV raising in the energy of the HOMO orbitals is observed, consistent with the electron–donating character of the methoxy and hydroxy group at position 3.

10.1002/anie.201912455
WILEY-VCH

RESEARCH ARTICLE

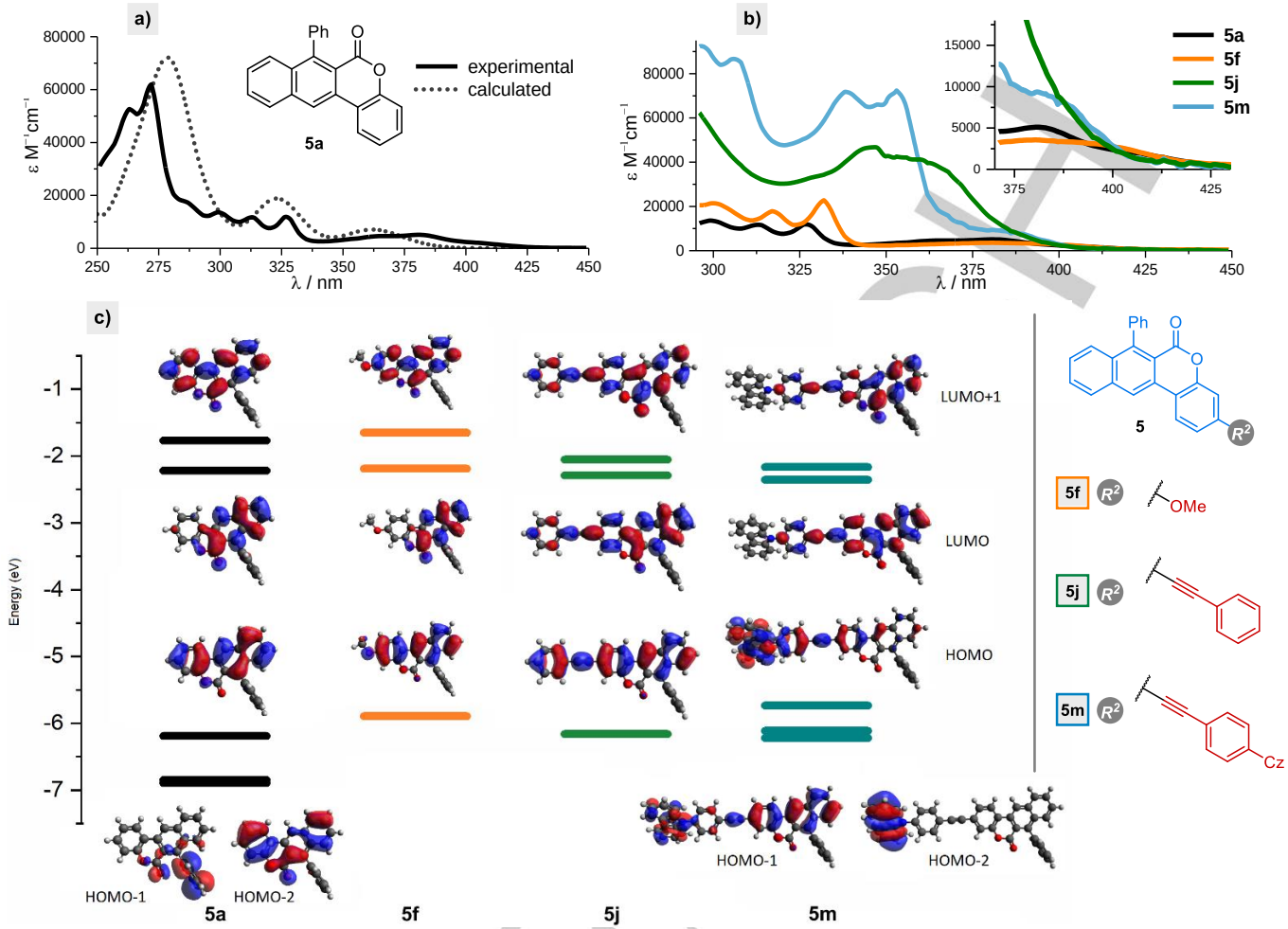

Figure 2. a) Measured and calculated absorption spectra of PC **5a**. b) Extinction coefficients of PC **5a**, **5f**, **5j** and **5m** measured in ACN. c) Selected frontier molecular orbitals of PC **5a**, **5f**, **5j** and **5m** and relative energies. Cz = carbazole.

The calculated absorption spectra of these PCs show a red shift to 387 and 385 nm for **5f** and **5g**, respectively, in agreement with the experimental values. A different scenario is observed by introducing conjugation at position 3. For PCs **5h**–**m** the extinction coefficient increases significantly (See **5j** and **5m** in Figure 2b). The presence of the triple bond significantly lowers the energy of the LUMO+1 orbital: moving from –1.77eV for **5a**, to –2.05 and –2.07 eV for **5j** and **5m** (Figure 2c). Thus, causing a red shift of the second less energetic transition at 323 for **5a**, to 371 and 387 nm for **5j** and **5m**, respectively. The further conjugation with a phenyl group increases the red shift of the absorption with a less energetic peak at 385–390 nm, this effect being ascribed to the increase in the HOMO energy. **5m** has the most red–shifted absorption (Figure 2b, azure line) ascribed to a distinctive HOMO higher in energy and located predominantly on the carbazole moiety, suggesting an intramolecular charge transfer contribution.

Excited state analysis. For organic PCs, the singlet excited state (S_1) is the most likely to react in bimolecular reactions to perform photoinduced electron transfer (PET).[15] Therefore, the S_1 characterization by its decay pathway and its lifetime, is instrumental to predict its reactivity.[15] High excited state energy means higher applications in a number of diverse PET reactions. Long lifetime will match with greater chances of encountering the desired reactant and the higher the fluorescence quantum yield, the greater the likelihood of PET happening.[6c] We started analysing **5a** looking at the modifications of S_1 properties caused by the different substitutions. PC **5a** has an emission maximum at 421 nm, consistent with an excited state energy of 3.29 eV, an emission quantum yield (QY) of 4% and an excited state lifetime of 1.44 ns (Table 2). Removing the phenyl ring in position 7 (**5c**) determines an emission shift of 10 nm to shorter wavelengths with an excited state energy of 3.35 eV, the highest in the series. The more compact core led to longer lifetime (3.86 ns) and higher QY (8%). While substitutions with electron withdrawing groups did not alter significantly the properties of **5**, PCs **5f** and **5g**, bearing electron–donating groups (Table 2), showed an increased QY to 12% for **5g** and to 20% for **5f** and a lifetime extension to 8.50 ns and 7.78 ns, respectively.

10.1002/anie.201912455

RESEARCH ARTICLE

Table 2. Excited– and Ground–State Photoredox Properties Summary.

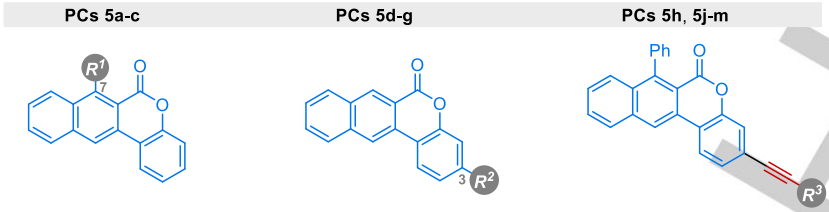

PC	λ_{max}em. (nm)	$E_{0,0}$ [a] (eV)	QY %	τ (ns)	E [b] (PC/PC•−)	E [b] (PC•+/PC)	E [b] (PC*/PC•−)	E [b] (PC•+/PC*)
5a, (R^1 = 7–Ph)	421	3.02	4	1.44	–1.74	1.75	1.28	-1.27
5b, (R^1 = 7–*o*–F)	421	3.15	9	2.07	–1.68	1.81	1.47	-1.34
5c, (R^1 = 7–H)	411	3.22	8	3.86	–1.67	1.80	1.55	-1.42
5d, (R^2 = 3–Br)	421	3.16	5	1.49	–1.61	1.78	1.55	-1.38
5e, (R^2 = 3–OTf)	413	3.20	4	0.81	–1.55	1.86	1.65	-1.34
5f, (R^2 = 3–OMe)	462	2.97	20	7.78	–1.76	1.47	1.21	-1.50
5g, (R^2 = 3–OH)	461	2.89	12	8.50	–1.89	1.44	1.00	-1.45
5h, (R^3 = TMS)	426	3.13	15	2.53	–1.71	1.73	1.42	-1.40
5j, (R^3= Ph)	434	3.12	17	3.34	–1.70	1.64	1.42	-1.48
5k, (R^3= *p*–CN–Ph)	427	3.14	23	3.05	–1.58	1.69	1.56	-1.45
5l, (R^3= *p*–OMe–Ph)	449	3.08	16	4.21	–1.65	1.44	1.43	-1.64
5m, (R^3= *p*–Cz–Ph)	459	3.12	6	2.49	–1.59	1.35	1.53	-1.77

[a] Estimated by emission onset at 77 K. [b] All potentials in V vs SCE. Measurements were performed in ACN (See SI). TMS = trimethylsilyl; Cz = carbazole.

Hence, these PCs are very good candidates towards demanding reductive PET processes. Finally, the increasing of the conjugation by a triple bond in compounds **5h**–**5m** also generated promising properties in between **5a** and **5f**–**5g**. The emission maximum was observed in a range from 427 nm (**5k**) to 459 nm (**5m**) with associated excited state energies between 3.18–3.23 eV. Quantum yield was observed in the range 15% mb – 23%, increased with respect to **5a**. The lifespan of the excited state was generally longer than 2 ns with a maximum for **5l** reaching 4.21 ns.

Redox properties analysis. One of the advantages of the NTs **5** is the associated wide redox window which allows both highly demanding reductive and oxidative quenching cycles. PC **5a** exhibited a reversible reduction at 1.75 V vs SCE ($PC^{\bullet+}$/PC) and an oxidation (PC/$PC^{\bullet-}$) at -1.74 V vs SCE. Moreover, the potentials of the excited states calculated 1.28 V (PC*/$PC^{\bullet-}$) and -1.27 ($PC^{\bullet+}$/PC*) are well suited for a variety of different photoreactions requiring strong oxidative or reductive power. Modulating the substituents within the NT core, it is possible to reach more negative values for E ($PC^{\bullet+}$/PC*) with electron donating groups in position 3, as in the case of **5f** with –1.50 V ang **5g** –1.45 V vs SCE. Even more highly negative values were registered for PCs with extended conjugation ranging from –1.45 V for **5k** up to a remarkable –1.77 V for **5m** (Table 2). Moving to the (PC*/$PC^{\bullet-}$) reductive process we immediately discern the wider variability of the PCs covering the window from 1.00 V for **5e** to 1.65 V for **5e**. As observed for the potential regarding ($PC^{\bullet+}$/PC*), the electron–donating ability of the substituents have a clear effect on the redox potentials, increasing the energy of the HOMO. Interestingly, addition of EWGs such as the case of **5b**, **5d**, **5e** and **5k** stabilizes the HOMO of the PCs bringing the potential above 1.65 V.

Analysis of the Photocatalytic Performances, Stability and Recyclability of the NT Photocatalysts. After having established general structure–property relationships across the 12 PCs, we first evaluated their photocatalytic performances with respect to the Povarov–type addition of *N,N*–dimethylaniline **6a** to phenylmaleimide **7** (Scheme 3). The choice of this photoreaction was made on the bases of three main considerations: (i) to relay on a well–known reaction mechanism where the PC is involved in two catalytic steps. The reported mechanism has been studied for both metal[16] and organic PCs,[17] facilitating comparisons; (ii) for the redox potential of **6a** (E_0 $\mathbf{6a}^{\bullet+}$/**6a** = +0.80 V vs SCE) and O_2 (E_0 $O_2/O_2^{\bullet-}$ = –0.64 V vs SCE),[19] which are within the operational windows of the 12 developed PCs, thus ensuring their comparison. and (iii) to assess the physicochemical stability of the NTs. The

10.1002/anie.201912455
WILEY-VCH

RESEARCH ARTICLE

presence of oxygen and hydrogen peroxide under basic conditions has been documented to be detrimental for the stability of different PCs.[18] As reported, the first step of the reaction (Scheme 3) involves a reductive quenching of the PC yielding its reduced form and the radical cation **9**.[20] Indeed, *N,N*–dimethylaniline **6** can efficiently quench **5***.

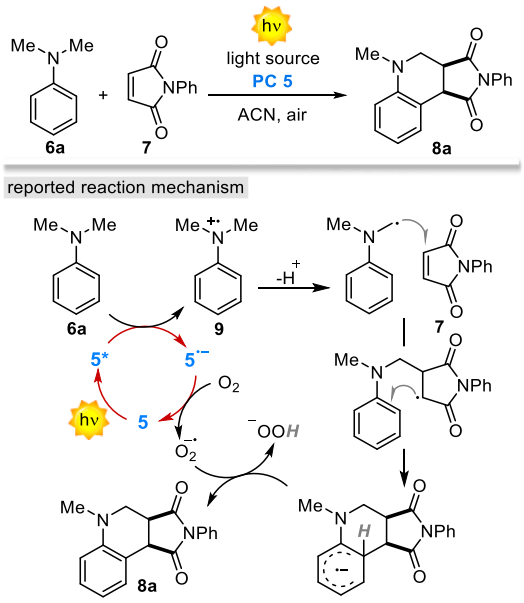

Scheme 3. Povarov–type addition of *N,N*–dimethylaniline **6a** to phenylmaleimide **7** – reported reaction mechanism.

The rate of this process was evaluated by Stern–Volmer plot (Figure 3). Considering a pure dynamic quenching, the slope (K_{PC}) of the Stern–Volmer plot is defined as: $K_{PC} = k_q \tau_{PC}$, where k_q is the bimolecular rate constant and τ_{PC} the excited state lifetime of the photocatalyst. Interestingly, the k_q of the different PCs **5** (Table S3 in SI) fall in a narrow range from 1.2 to 3.5 x 10^{10} $M^{-1}s^{-1}$, ascribable to diffusion-controlled processes. PCs **5f** and **5g**, having a τ of 7.78 and 8.5 ns, respectively, exhibited the steepest slopes. PCs with an extended conjugation such as **5h**–**5l** with a τ ranging from 2.53 to 4.21 ns also showed an efficient quenching. The trend was confirmed also considering the PCs with the shortest τ, such as **5d** and **5e**, which revealed the least efficient. A second indication was found with respect to the QY. All the PCs **5** with a quantum yield higher than 8% showed the fastest quenching. We next examined the photoredox performances of the 12 PCs in the Povarov–type reaction monitoring the yields of product **8a** after 24 h reaction time (Figure 4).[17] The best performing PCs were **5f** and **5g** which furnished the product **8a** in 91% and 86% yield (corresponding to 89% and 82% isolated yield, respectively) – in agreement with the quenching experiments. As predicted, also PCs **5l** showed excellent performances with 82% isolated yield (85% yield by GC-FID).

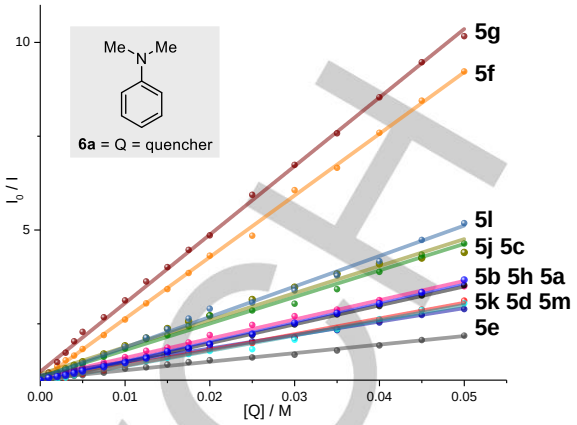

Figure 3. Stern–Volmer quenching between PCs **5** and *N,N*–dimethylaniline **6a** in ACN.

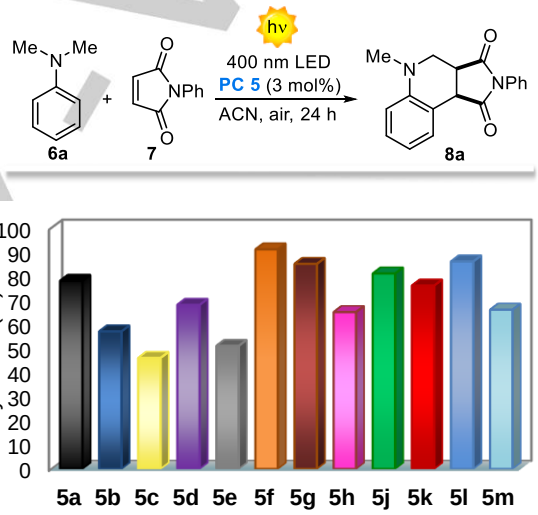

Figure 4. Observed performances of the PCs **5** for the reaction between *N,N*–dimethylaniline **6a** and phenylmaleimide **7**. Reported yields represent the media of two independent runs.

PCs **5a**, **5d**, **5j** and **5k** furnished the product in good yields spanning from 76% to 80%. In these cases, the fastest quenching is observed for **5j**, supported by Stern–Volmer experiments and reflected in a τ of 3.34 ns and a high extinction coefficient. The least performing PCs were **5e** and **5c**, with 51% and 46% yield, respectively. While **5e** performances were predicted by the lowest quenching constant of the series, **5c** performances were affected by the lowest absorption among the 12 PCs. Other PCs **5b**, **5d**, **5h** and **5m** gave average performances from 57% to 66% yield. It is worth mentioning that PC **5f** (89% yield) outperformed the previously reported yield values of eosin Y[17] and $Ru(bpy)_3$,[16] which furnished **8a** in 82% and 83% yield. At this point we evaluate the possibility of reuse our PCs over iterative photoreactions. An important issue related to the use of homogeneous PCs is the stability and recyclability of these

10.1002/anie.201912455

molecules. Gratefully, all the 12 PCs **5** were quantitatively recovered at the end of the reaction. Most importantly, recyclability studies performed on PC **5a** revealed the unique possibility of reuse the PC up to four times with negligible variations in its catalytic performances (Section F in SI).

Table 3. Observed performances of PCs **5** beyond the state–of–the–art synthetic applications.

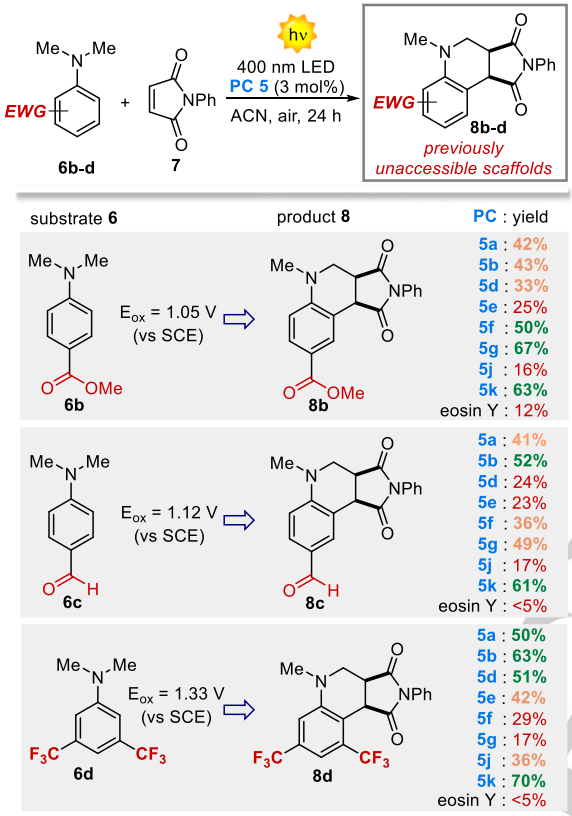

Next, we selected substrates **6b–d**, because of their high oxidation potentials (E_{ox} = 1.05–1.33 V vs SCE, see SI). Due to their thermodynamically demanding oxidations these compounds are beyond the state–of–the–art synthetic applications reported so far, catalysed by Ru–,[16] Cu–,[22] Co,[23] Ir,[24] Pt–complexes,[25] eosin Y[17] and different supported metal oxides including TiO_2.[26] In all these cases only halogens were partially tolerated as EWGs. When a different EWG was placed on the aromatic ring it completely shut down the reactivity of the system. We started using **6b**, bearing an ester group at the *p*–position (E_{ox} = 1.05 vs SCE). Two of the best performances were registered for **5f** and **5g**, with 50% and 67% yield respectively. Remarkably, the highly oxidant PC **5k** ($PC^*/PC^{\bullet-}$ = 1.56 V) furnished the product in 63% yield. Subsequently, **6c** was selected not only for the higher oxidation potential (E_{ox} = 1.12 V vs SCE), but also for the presence of an aldehyde moiety particularly sensitive to oxidative conditions. Gratefully, PCs **5b** and **5k**, characterized by high excited state reduction potentials delivered **8c** in 52% and 61% yield, respectively. Additional experiments were carried out with **6d** (E_{ox} = 1.33 vs SCE), bearing two CF_3 groups. The most oxidant PCs exhibited the best performances with **5k** furnishing **8d** in 70% yield. It is interesting to note how PCs **5f** and **5g** ($PC^*/PC^{\bullet-}$ = 1.21 and 1.00 V, respectively) showed inferior performances while moving from **6a–b** to the more oxidant substrate **6d**. This indicating an increased impact of the excited state oxidative power ($5^*/5^{\bullet-}$) while moving towards the thermodynamic oxidation limits of the PC. On the other hand, more oxidant PCs **5b** and **5k** ($PC^*/PC^{\bullet-}$ = 1.47 and 1.56 V) resulted in improved performances. Eosin Y, the previous PC of choice for this type of reactions, turned out completely inefficient. These experiments confirmed how the identification of novel PCs with wide redox windows can open the way to previously inaccessible substrates.

Synthetic Applications and Comparison of the Photocatalytic Performances. At this juncture, we decided to evaluate PCs **5** in diverse photochemical transformations. We started by testing their performances under reductive quenching methods, in the decarboxylative Giese–type addition between proline **9a** and dimethyl maleate **10** (Scheme 4). This reaction has been used as an evaluation probe for the synthetic performances of diverse photocatalytic systems, including: Ir–based PCs,[27] acridiniums[8c] and cyanoarenes.[6c] What makes this transformation difficult to be efficiently catalysed is the need of an optimal balance between the oxidative excited state properties of the PC and the reductive power of its radical anion. Thus ensuring: (i) an efficient decarboxylation step – with a PC* reductive quenching (**9b**–Cs E_{ox} = 0.95 V vs SCE)[27] –generating the reactive α–amino radical **12** and (ii) a fast reduction of the formed α–acyl radical **13** (E_{red} = – 0.60 V vs SCE)[27] – with a $PC^{\bullet-}$ oxidation step – which closes the photocatalytic cycle. It is worth mentioning that only specific Ir–based and organic PCs were able to catalyse this transformation.[8c,27] In fact, diverse PCs despite being characterised by competent redox potentials turned out highly inefficient. Interestingly, by using 5 mol% of **5a** and readily available CFL bulbs, the expected product **11** was obtained in 63% yield (Table 4, entry 1). Quite unexpectedly, PCs **5b** and **5d** furnished the product in reduced yields, 48% and 53%, respectively (Table 4, entries 2 and 3). Inferior results were obtained for **5e** (Table 4, entry 4), in agreement with his very short excited state lifetime of 0.81 ns (Table 1). PC **5f**, having inferior excited state oxidative power ($\mathbf{5f}^*/\mathbf{5f}^{\bullet-}$ = 1.21 V) and superior τ (7.78 ns) showed superior performances with 62% yield (Table 4, entry 5). Finally, PCs with an extended conjugation such as **5k** and **5m** efficiently catalysed this reaction with 75% and 70% yield, respectively. In particular **5k** with a $\mathbf{5k}^*/\mathbf{5k}^{\bullet-}$ = 1.65 and τ = 3.05 resulted the best of the series (Table 3, entry 6). Selected metal–based PCs were also compared under the same reaction conditions, with poor results (Table 3, entries 8–10).[27] To expand the repertoire of reaction catalysed by NTs with respect to reductive quenching, we explored a synthetically valuable light–driven acylation reaction (Table 5). The mechanism involves the oxidation of acylsilane **15** (E_{ox} = 1.46 V)[28] by **5***, generating after the silyl group cleavage the reactive acyl radical **19**. Trapping of **19** by crotonate **16** and

10.1002/anie.201912455
WILEY-VCH

RESEARCH ARTICLE

following reduction of radical **20** by **5**$^{\bullet -}$, delivers the β-ketoester **17**.

Table 4. Observed performances of PCs **5** for the Giese–type addition between **9** and dimethyl maleate **10**.

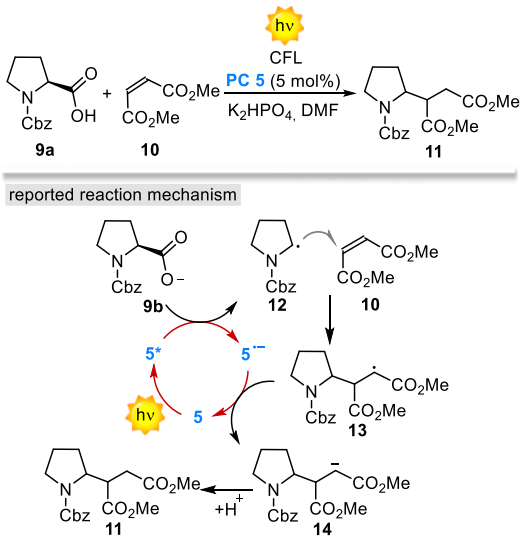

entry[a]	PC	yield %[b]
1	**5a**	66 (63)
2	**5b**	48
3	**5d**	53
5	**5f**	62
6	**5k**	77 (75)
7	**5m**	72 (70)
8	Ru(bpy)$_3$	<5
9	Ir(ppy)$_3$	<5
10	Ir(dFppy)$_3$	10
11[c]	Ir[dF(CF$_3$)ppy]$_2$(dtbbpy)+	93

[a] Reactions in DMF for 20h illuminated by CFL using PCs **5** (5 mol%), see SI. [b] Yields determined by ^{1}H NMR analysis of the crude mixture using trimethoxybenzene as internal standard. Isolated yields in parenthesis. [c] As reported in reference 27 (reaction time 36 h).

The reaction has significant thermodynamic restrictions. It is needed a PC oxidation potential > 1.46 V and a reduction potential < - 0.6 V.[27,28] Remarkably, different PCs **5** performed smoothly with **5k** (PC*/PC$^{\bullet -}$ = 1.56 V, PC$^{\bullet +}$/PC = -1.45 V) deliver the product in 85% yield. Metal-based and acridinium PCs revealed completely unproductive (entries 7-10). The only manner to access **17**, before the present report, was by using tutetrabutylammonium decatungstate (TBADT = nBu$_4$N)$_4$[W$_{10}$O$_{32}$]) PC under deep UV irradiation, 310 nm (60% yield).[28]

Table 5. Light–driven acylation of methyl crotonate **16**.

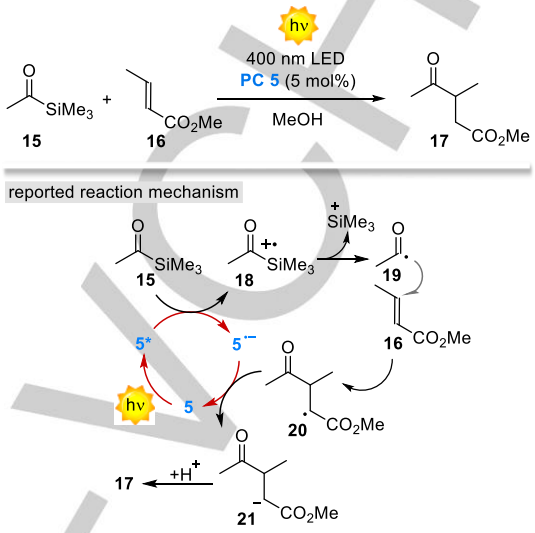

entry	PC	yield %
1	**5a**	69 (67)
2	**5b**	70
3	**5f**	66
4	**5g**	28
5	**5k**	88 (85)
6	**5m**	43
7	Ru(bpy)$_3$	-
8	Ir(ppy)$_3$	-
9	Acr$^+$-Mes	<5%
10[c]	TBADT @ 310 nm	60

[a] Reactions in MeOH at rt for 15h illuminated by LED using PCs **5** (5 mol%), see SI. [b] Yields determined by ^{1}H NMR analysis of the crude mixture using pyrazine as internal standard. In parenthesis isolated yields. [c] Result as in reference 28 (reaction time 8 h).

To further evaluate the generality of the PCs with respect to mechanistically reversed photochemical methods, we assessed them under oxidative quenching mechanisms. Hence, we selected diverse benzyl halides **22** (Table 6). Following previous reports on dehalogenation reactions,[29] we assumed the reaction to proceed through the single-electron reduction of **22** by **5***.[30] When PC **5a**, was irradiated under 400 nm light the benzyl iodide **22a** and benzyl bromide **22b** were efficiently reduced to the

10.1002/anie.201912455

corresponding toluene derivative **23** in 72% and 80% yield respectively (Table 6, entry 1 and 2).

Table 6. Observed performances of PCs **5** under direct light–driven dehalogenation reaction of benzyl halides **22a–c**.

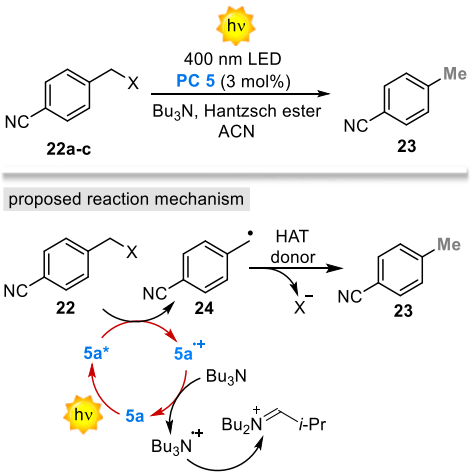

entry	15, X	E_{red} (V vs SCE)[b]	PC	yield
1	**22a**, I	–1.25	**5a**	82 (72)
2	**22b**, Br	–1.64	**5a**	82 (80)
3	**22b**, Br	–1.64	**5e**	9
4	**22b**, Br	–1.64	**5f**	68 (67)
5	**22b**, Br	–1.64	**5l**	62
6	**22b**, Br	–1.64	**5m**	46
7	**22c**, Cl	–1.81	**5a**	15
8	**22c**, Cl	–1.81	**5f**	48 (47)
9	**22c**, Cl	–1.81	**5l**	54 (51)
10	**22c**, Cl	–1.81	**5m**	48 (45)
11	**22c**, Cl	–1.81	$Ru(bpy)_3$	–
12	**22c**, Cl	–1.81	$Ir(ppy)_3$	<5
13	**22c**, Cl	–1.81	$Ir(dFppy)_3$	19

[a] Reactions in ACN at rt for 16 h under 400 nm LED strips using PCs **5** (3 mol%), see SI. [b] Yields determined by GC–FID analysis of the crude mixture using mesitylene as internal standard. In parenthesis isolated yields.

As expected, the less reductant PC **5e** showed much inferior results, while more electron–rich/more–reductant PCs **5f** and **5m** performed well, delivering **23** in 67% and 62% yield, respectively (Table 6, entries 4 and 5). We next examined benzyl chloride **22b** (E_{red} = –1.81 V vs SCE, See SI). Importantly, benzyl chlorides are generally unexpansive and readily available starting materials but their use in photocatalysis is often restricted by their difficult single–electron reduction. Notably, when the reaction was performed in the presence of **5a** product **23** formed in 15% yield. This prompted us to screen other PCs with respect to this unprecedented process. The most reducing PCs **5f**, **5l** and **5m** showed promising results, with 47%, 51% and 45% yield, respectively (Table 6, entries 8–10).

Table 7. Direct light–driven dehalogenation of methyl 4–iodobenzoate **25**.

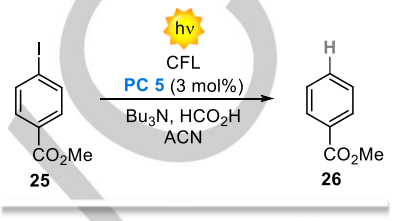

entry	PC	yield %
1	**5a**	86 (83)
2	**5d**	16
3	**5e**	13
4	**5f**	81
5	**5m**	96 (93)
6	$Ru(bpy)_3$	<5
7[c]	$Ir(ppy)_3$	92

[a] Reactions in ACN at rt for 20h under illumination by CFL using PCs **5** (3 mol%), see SI. [b] Yields determined by ^{1}H NMR analysis of the crude mixture using trimethoxybenzene as internal standard. Isolated yields in parenthesis. [c] Result as in reference 29 (reaction time 6 h).

The fact that only the most reductant PCs **5** were able to catalyse this reaction corroborates the reported oxidative quenching mechanism.[29] The difficulty of catalysing this reaction was confirmed with respect to diverse metal–based PCs (Table 6, entries 11–13). Only the highly reductant $Ir(dFppy)_3$ furnished the product to some extent (19% yield). It is worth mentioning that the only way to directly photo-generate this type of radicals starting from benzyl chlorides[31] is under deep–UV photochemistry.[32] Prompted by the results obtained for the reduction of benzylic chlorides, we next examined an additional oxidative-quenching-based reaction such as the deiodination of arenes. With methyl 4–iodobenzoate **25** (E_{red} = –1.96 V vs SCE, see SI) we further challenged the reductive excited state potential of our PCs. Interestingly, **5a** performed smoothly delivering **26** in 83% yield (Table 7, entry 1). Less reducing PCs, such as **5d** and **5e** gave **26** in poor yields (Table 7, entries 2 and 3). Contrarily, highly reducing PC **5f** and **5m** produced **26** in 81% and 93% yield, respectively (Table 7, entries 4 and 5), reaching the best results

obtained so far by more expanses rare Earth-metal complexes (entry 7). It should be noted that this type of reactions can be catalysed only by precious Ir–complexes[29] or trough consecutive visible light–induced electron transfer processes.[33] Thanks to their ambivalent oxidative/reductive nature the NT photocatalysts represent a new convenient option also towards the development of light-driven reductive methods.[34]

Conclusion

In conclusion, we have identified naphtochromenones as a new class of extremely versatile organic PCs. In fact, their wide redox window (up to 3.22 eV), is well distributed across highly energetic exited states potentials ranging from –1.77 V to 1.65 V. This unique feature of the NT photocatalysts ensures the access to both thermodynamically demanding oxidative and reductive light–driven transformations. Additional advantages are represented by the simple synthetic route developed, which allowed gram scale synthesis of the PCs (up to 2.88 g), making them affordable and sustainable. Furthermore, the NT core can be easily tuned, and the PCs can be recovered and reused maintaining comparable catalytic performances over four runs. Structure–property relationship, supported by DFT calculations, allows further uses towards the intended purpose. Finally, the synthetic potential of their dualistic properties was proven with five highly diverse photoreactions, characterised by strong and opposite thermodynamic requirements (from E_{ox} = 1.46 to E_{red} = –1.96 V), thus covering a vast applications spectrum. Interestingly, NTs outperformed diverse well–established PCs including eosin Y, acridinium, Ru– and Ir–complexes, while efficiently catalysing unprecedented Povarov-type reactions with electron-deficient dimethylanilines **6b-d** and photo-dehalogenation of benzyl chlorides **22c** (up to 70% and 51% yield, respectively). The merging of a redox window up to 3.22 eV, with an ambivalent oxidative/reductive nature, guarantees to NT photocatalysts the ability to unlocking previously inaccessible light–driven reactivity. Hence, their use will impart new directions to the growing field of photocatalysis.

Acknowledgements

This work was supported by the CariParo Foundation with the AMYCORES starting grant to L.D.. A. V.–P. thanks the Seal of Excellence @unipd PLACARD for a fellowship. AS thanks the University of Padova for the P–DiSC #10BIRD2018–UNIPD. Stefano Mercanzin, Mauro Meneghetti and Alberto Doimo are acknowledged for technical assistance.

Keywords: photoredox catalysis • organic catalyst • synthetic methods • light–driven reactions • radical chemistry

[1] a) L. A. Weinstein, J. Loomis, B. Bhatia, D. M. Bierman, E. N. Wang, G. Chen, *Chem. Rev.* **2015**, *115*, 12797–12838; b) J. Gong, C. Li, M. R. Wasielewski, *Chem. Soc. Rev.* **2019**, 48, 1862–1864; c) Y. Wang, H. Suzuki, J. Xie, O. Tomit, D. J. Martin, M. Higashi, D. Kong, R. Abe, J. Tang, *Chem. Rev.* **2016**, *116*, 9664–9682; d) G. J. Hedley, A. Ruseckas, D. W. Samuel, *Chem. Rev.* **2017**, *117*, 796–837.

[2] a) D. M. Schultz, T. P. Yoon, *Science*, **2014**, *343*, 1239176–1239184; b) D. Ravelli, D. Dondi, M. Fagnoni, A. Albini, *Chem. Soc. Rev.* **2009**, *38*, 1999–2011; c) L. Buzzetti, G. E. M. Crisenza, P. Melchiorre, *Angew. Chem. Int. Ed.* **2019**, *58*, 3730–374; d) *Angew. Chem. Int. Ed.* **2012**, 51, 6828–6838; e) *Acc. Chem. Res.* **2016**, 49, 1911–1923.

[3] a) J. C. Theriot, C. H. Lim, H. Yang, M. D. Ryan, C. B. Musgrave, G. M. Miyake, *Science*, **2016**, *352*, 1082–1086; b) N. Corrigan, S. Shanmugam, J. Xu, C. Boyer, *Chem. Soc. Rev.* **2016**, *45*, 6165–6212.

[4] a) L. Marzo, S. K. Pagire, O. Reiser, B. König, *Angew. Chem. Int. Ed.* **2018**, *57*, 10034–10072; *Angew. Chem.* **2018**, 130, 10188–10228; b) C. Michelin, N. Hoffmann, *Curr. Opin. Green Sustain. Chem.* **2018**, *10*, 40–45; c) T. Bach, P. Hehn, *Angew. Chem. Int. Ed.* **2011**, *50*, 1000–1045; *Angew. Chem.* **2011**, 123, 1032–1077.

[5] a) C. K. Prier, D. A. Rankic, D. W. C. MacMillan, *Chem. Rev.* **2013**, *113*, 5322–5363; b) A. Hossain, A. Bhattacharyya, O. Reiser, *Science*, **2019**, 364, eaav9713; c) M. H. Shaw, J. D. A. Twilton, D. W. C. MacMillan *J. Org. Chem.* **2016**, *81*, 6898–6926; d) R. C. McAtee, E. J. McClain, C. R. J. Stephenson, *Trends in Chemistry*, **2019**, *1*, 111–125; e) N. A. Romero, D. A. Nicewicz, *Chem. Rev.* **2016**, *116*, 10075–100166; f) K. L. Skubi, T. R. Blum, T. P. Yoon, *Chem. Rev.* **2016**, *116*, 10035–10074; g) D. P. Haria, B. König, *Chem. Commun.*, **2014**, *50*, 6688–6699.

[6] For selected recent examples see: a) R. M. Pearson, C.-H. Lim, S. M. Sartor, M. D. Ryan, H. Yang, N. H. Damrauer, G. M. Miyake. *Chem. Eur. J.* **2017**, *23*, 10962–10968; b) C. Bottecchia, R. Martín, I. Abdiaj, E. Crovini, J. Alcazar, J. Orduna, M. J. Blesa, J. R. Carillo, P. Prieto, T. Noël, *Adv. Synth. Catal.* **2019**, *361*, 945–950.

[7] For a recent example see e.g.: B. D. Ravetz, A. B. Pun, E. M. Churchill, D. N. Congreve, T. Rovis, L. M. Campos, *Nature* **2019**, *565*, 343–346.

[8] a) B. G. McCarthy, R. M. Pearson, C.−H. Lim, S. M. Sartor, N. H. Damrauer, G. M. Miyake, *J. Am. Chem. Soc.* **2018**, *140*, 5088−5101; b) M. Kim, S.–J. Yoon, S. H. Han, R. Ansari, J. Kieffer, J. Y. Lee, J. Kim, *Chem. Eur. J.* **2019**, *25*, 1829–1834; c) A. Joshi–Pangu, F. Lévesque, H. G. Roth, S. F. Oliver, L.–C. Campeau, D. A. Nicewicz, D. A. DiRocco, *J. Org. Chem.* **2016**, *81*, 7244–7249; d) E. Alfonzo, F. S. Alfonso, A. B. Beeler, *Org. Lett.* **2017**, *19*, 2989–2992; e) E. Speckmeier, T. G. Fischer, K. Zeitler, *J. Am. Chem. Soc.* **2018**, 140, *45,* 15353–15365; f) J. Lu, B. Pattengale, Q. Liu, S. Yang, W. Shi, S. Li, J. Huang, J. Zhang, *J. Am. Chem. Soc.* **2018**, 140, *45,* 13719–13725; g) F. Le Vaillant, M. Garreau, S. Nicolai, G. Gryn'ova, C. Corminboeuf, J. Waser, *Chem. Sci.* **2018**, *9*, 5883–5889; h) M. Garreau, F. Le Vaillant, J. Waser, *Angew. Chem. Int. Ed.* **2019**, *58*, 8182–8186.

[9] a) J. Mateos, A. Cherubini–Celli, T. Carofiglio, M. Bonchio, N. Marino, X. Companyó, L. Dell'Amico, *Chem. Commun.* **2018**, *54*, 6820–6823; b) J. Mateos, N. Meneghini, M. Bonchio, N. Marino, T. Carofiglio, X. Companyó, L. Dell'Amico, *Beilstein J. Org. Chem.* **2018**, *14*, 2418–2424.

[10] a) L. Dell'Amico, A. Vega–Peñaloza, S. Cuadros, P. Melchiorre, *Angew. Chem. Int. Ed.* **2016**, *55*, 3313–3317; *Angew. Chem.* **2016**, 128, 3374 – 3378; b) L. Dell'Amico, V. M. Fernández–Alvarez, F. Maseras, P. Melchiorre, *Angew. Chem. Int. Ed.* **2017**, *56*, 3304–3308; *Angew. Chem.* **2017**, 129, 3352–3356; c) S. Cuadros, L. Dell'Amico, P. Melchiorre, *Angew. Chem. Int. Ed.* **2017**, *56*, 11875–11879.

[11] For the photochemistry of benzophenone and its derivatives see: a) D. Ravelli, S. Protti, M. Fagnoni, *Chem. Rev.* **2016**, *116*, 9850–9913. For the photochemistry of coumarins see e.g.: b) A. Gualandi, G. Rodeghiero, E. Dell Rocca, F. Bertoni, M. Marchini, R. Perciaccante, T. P. Jansen, P. Ceroni, P. G. Cozzi, *Chem. Commun.* **2018**, *51*, 10044–10047.

[12] The latter oxidative aromatization step is driven by the presence of oxygen. Control experiments performed under a nitrogen atmosphere furnished only the elimination product of type **4**.

[13] This functional allowed a good match of the calculated and experimental absorption spectra. See: T.M. McCormick, C. R. Bridges, E. I. Carrera, P. M. DiCarmine, G. L. Gibson, J. Hollinger, L. M. Kozycz, D. S. Seferos, *Macromolecules*, **2013**, *46*, 10, 3879–3886.

[14] The plane of the phenyl ring forms a 90° dihedral angle with the plane described by the NT scaffold, hampering its direct conjugation.

[15] For all the 12 PC **5** we have calculated the T_1 excited states energy and the corresponding lifetimes (section C in SI). The resulting T_1 potentials are unable to drive the reactions herein discussed (*vide infra*). In agreement with the lower T_1 excited state potentials, compound **6a** and **7** were not able to quench **5a*** T_1, ruling out the hypothesis of T_1 catalysed processes. See: V. Balzani, P. Ceroni, A. Juris, *Photochemistry and Photophysics: Concepts, Research, Applications*, 1st ed.; Wiley–VCH: Weinheim, **2014**.

[16] X. Ju, W. Li, W. Yu, F. Bian, *Adv. Synth. Catal.* **2012**, *354*, 3561–3567.

[17] Z. Liang, S. Xu, W. Tian, R. Zhang, *Beilstein J. Org. Chem.* **2015**, *11*, 425–430.

[18] a) G. Oster, N. Wotherspoon, *J. Chem. Phys.* **1954**, *22*, 157–158; b) M. Majek, F. Filace, J. A. von Wangelin, *Beilstein J. Org. Chem.* **2014**, *10*, 981–989.

[19] P.S. Singh, D. H. Evans, *J. Phys. Chem. B*, **2006**, *110*, 637–644.

[20] Stern–Volmer quenching experiments indicate that also phenylmaleimide **7** can quench **5a***. Control experiments were performed in the presence of an excess of maleimide **7** (2 and 5 eq.). In these cases, the yields dropped significantly from 78% to 22% and 15%, respectively. Hence, the quenching of **5*** by **7** leads to an unproductive pathway.

[21] J. R. Lakowicz, *Principles of Fluorescence Spectroscopy*, 3rd ed.; Springer: Boston, **2010**.

[22] T. P. Nicholls, G. E. Constable, J. C. Robertson, M. G. Gardiner, A. C. Bissember *ACS Catal.* **2016**, *6*, 451–457.

[23] X.–L. Yang, J.–D. Guo, T. Lei, B. Chen, C.–H. Tung, L.–Z. Wu, *Org. Lett.* **2018**, *20*, 2916–2920.

[24] F. Peng, P. Zhi, H. Ji, H. Zhao, F.–Y. Kong, X.–Z. Liang, Y.–M. Shen, *RSC Adv.* **2017**, 7, 19948–19953.

[25] A. M. Ranieri, L. K. Burt, S. Stagni, S. Zacchini, B. W. Skelton, M. I. Ogden, A. C. Bissember, M. Massi, *Organometallics,* **2019**, *38*, 1108–1117.

[26] J. Tang, G. Grampp, Y. Liu, B.–X. Wang, F.–F. Tao, L.–J. Wang, X.–Z. Liang, H.–Q. Xiao, Y.–M. J. Shen, *J. Org. Chem.* **2015**, *80*, 2724–2732.

[27] L. Chu, C. Ohta, Z. Zuo, D. W. C. MacMillan, *J. Am. Chem. Soc.* **2014**, *136*, 10886–10889.

[28] L. Capaldo, R. Riccardi, D. Ravelli, M. Fagnoni, *ACS Catal.* **2018**, *8*, 304−309.

[29] J. D. Nguyen, E. M. D'Amato, J. M. R. Narayanam, C. R. J. Stephenson, *Nat. Chem*. **2012**, *4*, 854–859.

[30] Stern–Volmer experiments indicate that **5a*** is quenched by both the benzyl halide and the amine. The ambivalent oxidative and reductive powers of the developed PCs **5** allow both reductive and oxidative quenching cycles to be operative with definite advantages for the overall reactivity of the system (Figure S125-126 in SI).

[31] An indirect nucleophilic approach has been recently reported. See: B. Schweitzer–Chaput, M. A. Horwitz, E. de Pedro Beato, P. Melchiorre, *Nat. Chem.* **2019**, *11*, 129–135.

[32] a) J. Bonin, C. Costentin, M. Mahet, J.–B. Mulon, M. Robert, *Phys. Chem. Chem. Phys*. **2009**, *11*, 10275–10280; b) G. Qiu, Y. Li, J. Wu, *Org. Chem. Front.* **2016**, *3*, 1011–1027.

[33] I. Ghosh, T. Ghosh, J. I. Bardagi, B. König, *Science* **2014**, **346**, 725–728.

[34] Slightly differences from the required reduction potentials are possibly compensated by the irreversible formation of the aromatic radical and the iodide anion. For a discussion see: a) I. Ghosh, R. S. Shaikh, B. König, *Angew. Chem. Int. Ed.* **2017**, *56*, 8544–8549; *Angew. Chem.* **2017**, 129, 8664–8669; b) M. Marchini, G. Bergamini, P. G. Cozzi, P. Ceroni, V. Balzani, *Angew. Chem. Int. Ed.* **2017**, *56*, 12820–12821; *Angew. Chem.* **2017**, 129, 12996–12997; c) I. Ghosh, J. I. Bardagi, B. König, *Angew. Chem. Int. Ed.* **2017**, 56, 12822–1282; *Angew. Chem*. **2017**,129, 12998–1300.

10.1002/anie.201912455

WILEY-VCH

RESEARCH ARTICLE

Entry for the Table of Contents (Please choose one layout)
Layout 2:

RESEARCH ARTICLE

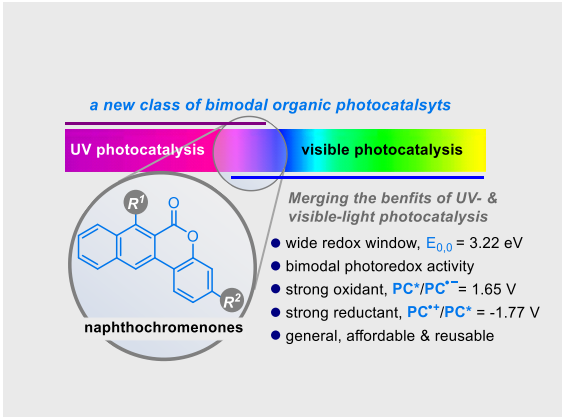

*Javier Mateos, Francesco Rigodanza, Alberto Vega–Peñaloza, Andrea Sartorel, Mirco Natali, Tommaso Bortolato, Giorgio Pelosi, Xavier Companyó, Marcella Bonchio, and Luca Dell'Amico**

Page No. – Page No.
Naphthochromenones: Organic Bimodal Photocatalysts Engaging in Both Oxidative and Reductive Quenching Processes.